

# MULTI-RADAR MULTI-SENSOR (MRMS) QUANTITATIVE PRECIPITATION ESTIMATION

## Initial Operating Capabilities

BY JIAN ZHANG, KENNETH HOWARD, CARRIE LANGSTON, BRIAN KANEY, YOUCUN QI, LIN TANG,  
HEATHER GRAMS, YADONG WANG, STEPHEN COCKS, STEVEN MARTINAITIS, AMI ARTHUR, KAREN COOPER,  
JEFF BROGDEN, AND DAVID KITZMILLER

The initial operating capabilities of the Multi-Radar Multi-Sensor quantitative precipitation system include an ensemble of quantitative precipitation estimations and associated diagnostic products based on radar, gauge, and atmospheric environmental and climatological data at 1-km resolution and a 2-min update cycle over the conterminous United States.

Over the last two decades, there has been a focus on developing new applications and systems to address requirements for seamless national radar information for use in model data assimilation, transportation, and quantitative precipitation

estimation, which integrate multiple overlapping radars with other in situ or remote sensing observations and numerical weather prediction (NWP) model output. Advances in computational speed and expanding Internet bandwidth facilitated the ability to move radar base data from single radars into regional and national centers for processing (Droegemeier et al. 2002; Kelleher et al. 2007).

The Multi-Radar Multi-Sensor (MRMS) system recently implemented at the National Centers for Environmental Prediction (NCEP) demonstrated such capabilities. MRMS currently integrates about 180 operational radars and creates a seamless 3D radar mosaic across the conterminous United States (CONUS) and southern Canada at very high spatial (1 km) and temporal (2 min) resolution. The radar base data are integrated with atmospheric environmental data, satellite data, and lightning and rain gauge observations to generate a suite of severe weather and quantitative precipitation estimation (QPE) products. Multiradar integration can mitigate deficiencies in the single-radar framework

**AFFILIATIONS:** ZHANG AND HOWARD—NOAA/OAR/NSSL, Norman, Oklahoma; LANGSTON, KANEY, QI, TANG, GRAMS, WANG, COCKS, MARTINAITIS, ARTHUR, COOPER, AND BROGDEN—NOAA/OAR/NSSL, and Cooperative Institute for Mesoscale Meteorological Studies, University of Oklahoma, Norman, Oklahoma; KITZMILLER—NOAA/NWS/OHD, Silver Spring, Maryland

**CORRESPONDING AUTHOR:** Jian Zhang, NSSL, National Weather Center, 120 David L. Boren Blvd., Norman, OK 73072  
E-mail: jian.zhang@noaa.gov

*The abstract for this article can be found in this issue, following the table of contents.*

DOI:10.1175/BAMS-D-14-00174.1

In final form 23 July 2015

©2016 American Meteorological Society

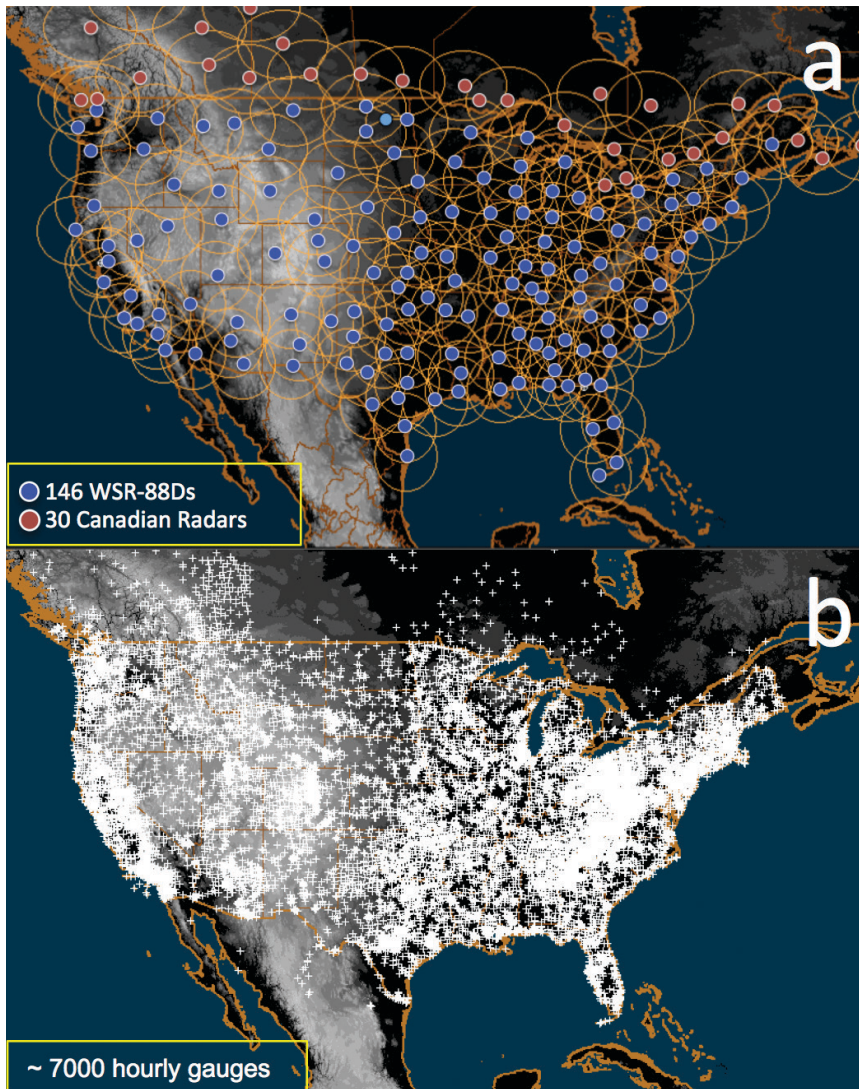


**FIG. 1. MRMS domain and locations of the (a) radar and (b) rain gauge sites. In (a), the blue dots indicate the U.S. WSR-88D radar sites, the maroon dots indicate the Canadian radar sites, and the brown circles are the 250-km range rings. The white plus signs in (b) indicate locations of the hourly gauges.**

(e.g., “cone of silence”). The integration of radar with multisensor data provides more accurate diagnoses of physical processes in the atmosphere than using radar data alone. For instance, the 3D temperature and moisture field is very helpful in hydrometeor classifications and segregation of continental and tropical rain.

MRMS was conceived and built at the National Severe Storms Laboratory (NSSL) using components from the Warning Decision Support System–Integrated Information (WDSS-II; Lakshmanan et al. 2007) and National Mosaic and Multi-Sensor QPE (NMQ) (Zhang et al. 2011) systems. The MRMS severe weather algorithms are derived using WDSS-II, and MRMS QPE algorithms are largely based on the NMQ

QPE components. The following paper provides an overview of the initial operating capabilities (IOC) of MRMS QPE products. An overview of the MRMS severe weather products will be presented in a separate paper (Smith et al. 2016).

### MRMS QPE DOMAIN.

The MRMS CONUS domain covers an area with latitude bounds of 20° and 55°N and longitude bounds of 130° and 60°W (Fig. 1). The MRMS grid has a horizontal resolution of 0.01° in both latitude and longitude directions, which is equivalent to about 1.11 km in the north–south direction throughout the domain. In the west–east direction, the grid resolution varies from about 1 km at the southern bound to about 0.6 km at the northern bound.

### MRMS QPE INPUT DATA.

**Radar.** MRMS ingests 3D volume scan data from about 146 S-band dual-polarization Weather Surveillance Radar-1988 Doppler (WSR-88D) radars and about 30 C-band single-polarization weather radars operated by Environment

Canada (Fig. 1a). The volume scan duration from these networks ranges from 3 to 10 min. A dual-polarization radar quality control (dpQC; Tang et al. 2014) is applied to WSR-88D data to remove nonhydrometeor echoes. The dpQC uses a simple correlation coefficient ( $\rho_{HV}$ ) filter that separates hydrometeor (high  $\rho_{HV}$ ; Fig. 2) and nonhydrometeor (low  $\rho_{HV}$ ; Fig. 2) areas and a set of heuristic rules that handles exceptions to the simple  $\rho_{HV}$  filter. Such exceptions include areas of hail, nonuniform beamfilling (NBF), and melting layer (ML) that have low  $\rho_{HV}$  values. Another exception is random clutter and biological pixels with high  $\rho_{HV}$  values. The dpQC uses 3D reflectivity structure and environmental data to protect hail, NBF, and ML areas

from being removed by the simple  $\rho_{HV}$  filter, and it uses spatial filters and vertical and horizontal consistency checks to remove random nonprecipitation pixels that exhibit high  $\rho_{HV}$  values. The dpQC removes more than 99% of nonhydrometeor echoes with very high computational efficiency (Tang et al. 2014). Wind farms (WF), anomalous propagation (AP) ground clutter, and deep biological echoes (“blooms”; Figs. 3a and 3c) were major challenges for the single-polarization radar QC, but those nonhydrometeor echoes are remarkably reduced in the dpQC (Figs. 3b and 3d). The WF and AP embedded in precipitation remain an issue and a WF mitigation scheme is currently under development. The WF locations are manually tabulated from available WF databases (e.g., Diffendorfer et al. 2014) and are based on “hot spots” in precipitation accumulations, and an aggressive dpQC will apply in the vicinity of WF. The WF mitigation is planned for implementation in the operational MRMS system later in 2016. It is noted that because of the hybrid polarization scheme, the horizontally polarized transmit power of WSR-88D radars is about 3 dB lower than it was before the polarimetric upgrade. Therefore, the radar may have less detection of light precipitation and snow than before, especially at long ranges.

The Canadian radar data used in MRMS are the full 3D volume scan (“CONVOL”) base-level data that contain 24 tilts with the lowest elevation angles ranging from  $-0.5^\circ$  to  $0.3^\circ$  and the highest at about  $24.6^\circ$ . Since the CONVOL dataset does not contain velocity and spectrum data, its quality control is mostly based on reflectivity structure. Two main processes are applied to remove nonprecipitation echoes: 1) a neural network-based reflectivity quality control (QC) with a static clutter map filter to remove persistent ground clutter (Lakshmanan et al. 2012) and 2) a heuristic rule-based AP removal using reflectivity intensity, echo depth, vertical gradient, and horizontal texture. Because of the low elevation angles, significant normal or AP ground clutter occurs in Canadian radar observations. Current QC measures remove persistent ground clutter and AP in clear air relatively effectively (Fig. 4). However, AP at far ranges and AP

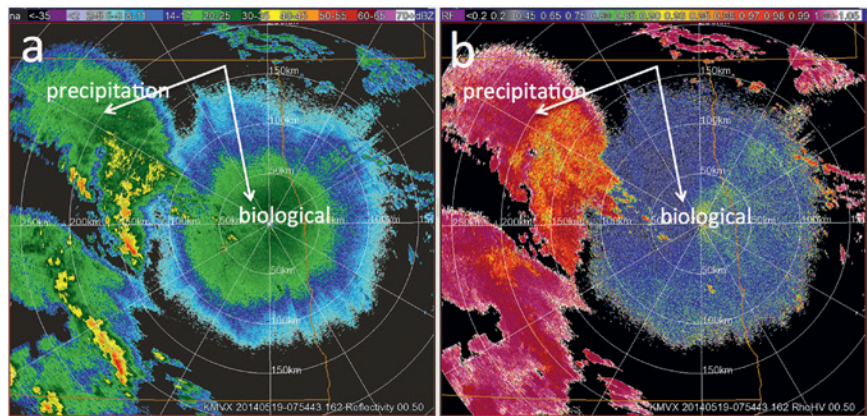


**FIG. 2.** (a) Base reflectivity and (b) correlation coefficient fields from the KMXV radar  $0.5^\circ$  tilt valid at 0800 UTC 19 May 2014. White circles are range rings at 50-km intervals, and white lines indicate azimuths every  $45^\circ$ . The white arrows indicate an area of precipitation to the northwest and an area of bird and insect echoes around the radar. The two areas have very similar reflectivity features as shown in (a) but distinctively different correlation coefficients as shown in (b).

embedded in precipitation remain a challenge owing to limited single-polarization radar information. Attenuation is another potential issue with Canadian radar data given their 5-cm wavelength. Currently no attenuation correction is applied in MRMS. Despite the remaining AP and attenuation issues, Canadian radar data are included in the MRMS products since they provide valuable information about distributions of storms and precipitation along the U.S.–Canada border. Such information is important for aviation and hydrological communities. There is a plan to begin upgrading the Canadian radar network with polarimetric capabilities in the next couple of years (P. Joe, Environment Canada, 2015, personal communication), and mitigations of AP and attenuation are expected to improve significantly with the upgrade.

**Gauge.** MRMS ingests approximately 7,000 hourly rain gauges from the Hydrometeorological Automated Data System (HADS; [www.nws.noaa.gov/oh/hads/](http://www.nws.noaa.gov/oh/hads/)) (Fig. 1b). Gauge data are the only operational in situ measurements of precipitation and are used to correct radar QPE biases in MRMS. However, gauge data are subject to many error sources that have been documented for decades (e.g., Parsons 1941; Larson and Peck 1974; Essery and Wilcock 1991; Groisman and Legates 1994; Sevruk 2005; Sieck et al. 2007; Rasmussen et al. 2012) and quality control of the data is necessary.

The hourly HADS gauges used in MRMS are quality controlled through an automated scheme that compares each gauge report with collocated hourly radar QPE values. Five types of suspicious gauges

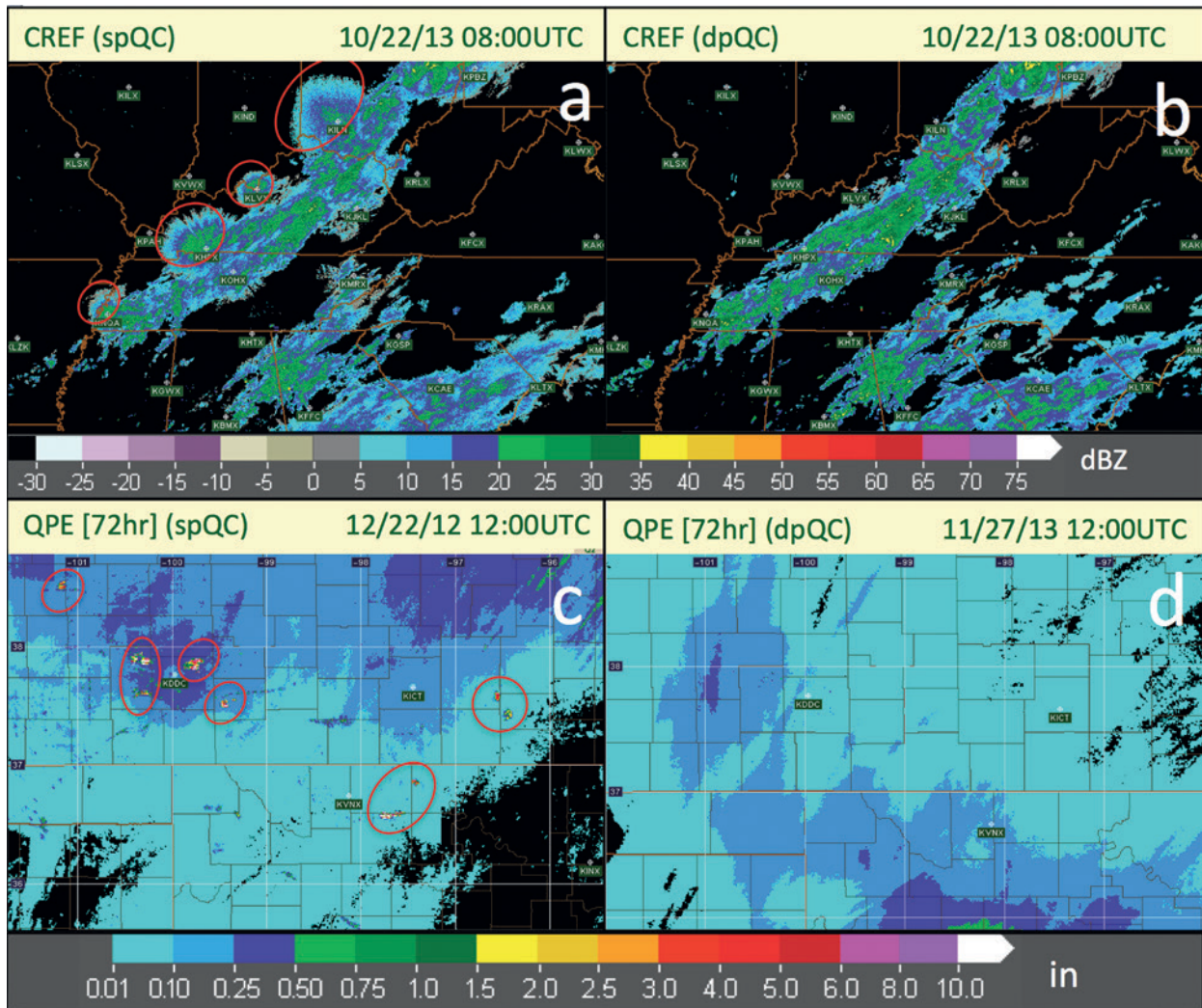


**FIG. 3.** (a),(b) Mosaicked composite reflectivity fields at 0000 UTC 22 Oct 2013 across the east-central United States. (c),(d) The 72-h radar QPE accumulations along the Oklahoma–Kansas border ending at 1200 UTC 22 Dec 2012 and 27 Nov 2013, respectively. The fields in (a) and (c) are from single-polarization radar reflectivity QC, and the fields in (b) and (d) are from dpQC. The red circles indicate biological echoes in (a) and WF in (c).

are identified, which are “frozen,” “false zero,” “false precipitation,” “outlier too high,” and “outlier too low.” The majority of the HADS gauges is tipping-bucket type and was found to be incapable of measuring frozen precipitation properly even when heated (e.g., Rasmussen et al. 2012). Therefore, gauges that report zero precipitation while the collocated radar QPE is greater than zero are labeled “frozen” when the surface wet-bulb temperature (WBT) is at or below 0°C. Further, all gauge data that report nonzero precipitation when  $WBT \leq 0^\circ\text{C}$  are also considered unreliable and are labeled “frozen” to avoid reports of partially melted frozen precipitation. A false-zero gauge is identified when a zero gauge report is collocated with a nonzero radar QPE, and a false-precipitation gauge is identified when the opposite occurs. This check

effectively identifies “stuck” gauges that report constant zero and gauges that report false precipitation in a clear-air environment, such as unheated gauges reporting precipitation from thawing snow after the precipitation has ended. Outlier-too-high and outlier-too-low gauges are identified when the reports are outside a predefined range around the hourly radar QPE. The range is from  $0.045R^{1.45}$  to  $1.0 + 6.4R^{0.725}$  [where  $R$  is the hourly radar QPE (in mm)] and retains about 95.8% of the good data and removes about 74% of the bad data based on a test with several thousands of manually quality-controlled data. In areas with poor radar coverage, a sanity check flags any hourly gauge report greater than 2 in. (50.8 mm) as suspicious. The current gauge QC does not contain spatial and temporal consistency checks but such schemes are evaluated

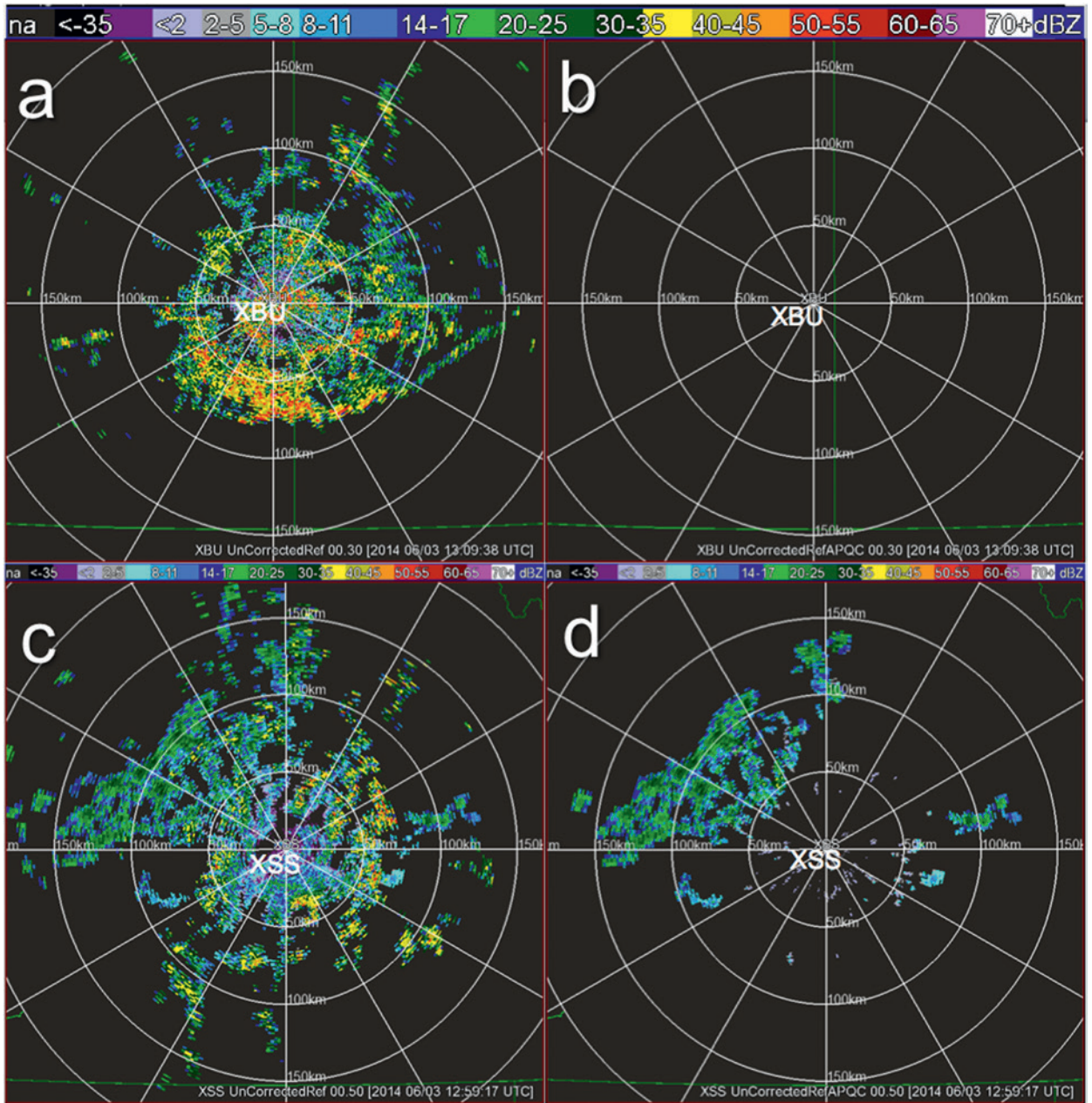


**FIG. 4. Base reflectivity at 0.5° tilt (a),(c) before and (b),(d) after the Canadian radar QC process. The fields were observed from (a),(b) XBU radar (Schuler, Alberta, Canada) valid at 1309:38 UTC and (c),(d) XSS radar (Silver Star Mountain, British Columbia, Canada) at 1259:17 UTC 3 Jun 2014.**

for various precipitation events and may be included in future updates. Nevertheless, the gauge QC provides a way to process large datasets and to remove significantly bad gauges effectively. The quality-controlled gauge data are used in the MRMS local gauge bias-corrected radar QPE that will be presented later in the paper.

**NWP model data.** Hourly analyses from the Rapid Refresh (RAP; <http://rapidrefresh.noaa.gov>) model have been used extensively in MRMS. For instance,

the RAP freezing-level height is used in the dpQC to help delineate areas of melting layer. Surface temperature and wet-bulb temperature are used to delineate areas of snow and rain. The RAP 3D temperature, wind, and relative humidity fields provide information about different atmospheric environments that may or may not be favorable for enhanced precipitation rates. High-Resolution Rapid Refresh (HRRR; <http://ruc.noaa.gov/hrrr/>) model data are planned to replace RAP as inputs to MRMS by the end of 2016.

**Precipitation climatology.** A special dataset of monthly precipitation climatology is utilized in MRMS for a gauge-and-climatology-merged QPE called “Mountain Mapper” (Schaake et al. 2004). The climatology is from the Parameter-Elevation Regressions on Independent Slopes Model (PRISM; Daly et al. 2008, 1994; [www.prism.oregonstate.edu](http://www.prism.oregonstate.edu)), which is derived using 30 years of gauge observations, atmospheric environmental data, and terrain elevation information. The PRISM monthly climatology captures the orographic forcing of precipitation in complex terrain and can provide a high-resolution background precipitation distribution when radar coverage is poor (e.g., in the Intermountain West; Maddox et al. 2002). PRISM has been used in several River Forecast Centers (RFCs) in the west for their operational precipitation estimation and river flow forecasts. The same process is adopted in MRMS to generate a CONUS Mountain Mapper QPE.

**MRMS QPE PRODUCTS.** MRMS currently provides four types of QPE products: 1) radar-based QPE, 2) gauge-based QPE, 3) local gauge bias-corrected

radar QPE, and 4) gauge-and-precipitation-climatology-merged QPE. Each QPE includes a suite of accumulations ranging from 1 to 72 h. The QPE products are generated operationally at NCEP and disseminated to the National Weather Service (NWS) regional and local forecast offices as well as external users and agencies. For instance, MRMS radar-based QPE products have been used by several RFCs in the eastern United States to create their operational river flow predictions. Table 1 summarizes the key QPE products in MRMS and the rest of the paper provides brief descriptions of each product.

**Seamless hybrid scan reflectivity and the associated height.** Radar QPEs are usually derived from the lowest radar bins that are not severely blocked. Reflectivity data from those radar bins constitutes the so-called hybrid scan reflectivity (HSR) (e.g., Fulton et al. 1998), and it forms the basis for the radar precipitation estimation and for extrapolation to the ground. The standard hybrid scan is constructed based on terrain data assuming radar beam propagation in standard atmosphere. The QPEs derived from

**TABLE 1. List of key MRMS precipitation products.**

ID	Unit	Update cycle	Description
SHSR	dBZ	2 min	SHSR
SHSRH	km AGL	2 min	Height of SHSR
RQI	—	2 min	RQI
POWR	—	1 h	Probability of warm rain
PCP_FLAG	—	2 min	Surface precipitation type
PCP_RATE	mm h <sup>-1</sup>	2 min	Surface precipitation rate
Q3RAD_SHSR_1H	mm	2 min	Radar-based 1-h precipitation accumulations
Q3RAD_SHSR_3 (6, 12, 24)H	mm	1 h	Radar-based 3 (6, 12, 24)-h precipitation accumulations
Q3RAD_SHSR_48 (72)H	mm	Daily at 1200 UTC	Radar-based 48 (72)-h precipitation accumulations
Q3GC_SHSR_1 (3, 6, 12, 24)H	mm	1 h	1 (3, 6, 12, 24)-h local gauge bias-corrected radar precipitation accumulations
Q3GC_SHSR_48 (72)H	mm	Daily at 1200 UTC	48 (72)-h local gauge bias-corrected radar precipitation accumulations
GII	—	1 h	GII
Q3GAUGE_1 (3, 6, 12, 24)H	mm	1 h	1 (3, 6, 12, 24)-h gauge-based precipitation accumulations
Q3GAUGE_48 (72)H	mm	Daily at 1200 UTC	48 (72)-h gauge-based precipitation accumulations
Q3MM_1 (3, 6, 12, 24)H	mm	1 h	1 (3, 6, 12, 24)-h Mountain Mapper precipitation accumulations
Q3MM_48 (72)H	mm	Daily at 1200 UTC	48 (72)-h Mountain Mapper precipitation accumulations

standard HSR often exhibit discontinuities from blockages not accounted for in the terrain data (e.g., those from man-made towers and growing trees). In MRMS, such gaps are identified from precipitation accumulation maps (Tang et al. 2013) and a linear cross-azimuth interpolation is applied to fill in small gaps (e.g., Fig. 5b vs Fig. 5a). Large gaps ( $\geq 5^\circ$ ) are filled with data from the next upper tilt (Fig. 5d vs Fig. 5c). The resultant HSR field is called “seamless” HSR (SHSR).

An apparent vertical profile of reflectivity (AVPR) correction (Zhang and Qi 2010; Zhang et al. 2012b; Qi et al. 2013a,b) is applied in the SHSR field to mitigate radar QPE overestimation errors in the “bright band” (BB) zone, where radar beams intersect the melting layer. AVPR refers to a radial profile of azimuthal mean reflectivities in stratiform rain areas in a given tilt where the radar beam is potentially intersecting or overshooting a melting layer. Assuming that the vertical structure of precipitation is horizontally uniform in the stratiform rain, the AVPR represents the vertical variation of reflectivity manifested by

the beam broadening effect (thus the term “apparent” VPR). Example AVPRs from KLWX (Sterling, Virginia) observations during Hurricane Sandy are shown in Fig. 6. Each AVPR of a given tilt is fitted with a three-piece (i.e., above BB top, BB top to peak, and BB peak to bottom) linear model. Assuming the precipitation rate below the BB bottom is constant, the linear AVPRs show that reflectivities in (above) the BB are higher (lower) than the reflectivity at the BB bottom (Fig. 6) and would result in overestimation (underestimation) errors if the reflectivities were used in the radar QPE without any correction. Figure 7 shows example 24-h radar QPEs from KLWX before and after the AVPR correction during Hurricane Sandy. The overestimation is apparent in an area west of the radar (blue circles in Fig. 7b), which resulted in a high Q/G ratio (1.75) when compared to gauge observations, where Q represents the radar QPE amount and G represents the gauge-observed amount. After the correction, the ratio was reduced to 1.07 and the root-mean-square error was reduced by about 58% (Fig. 7c vs Fig. 7f).

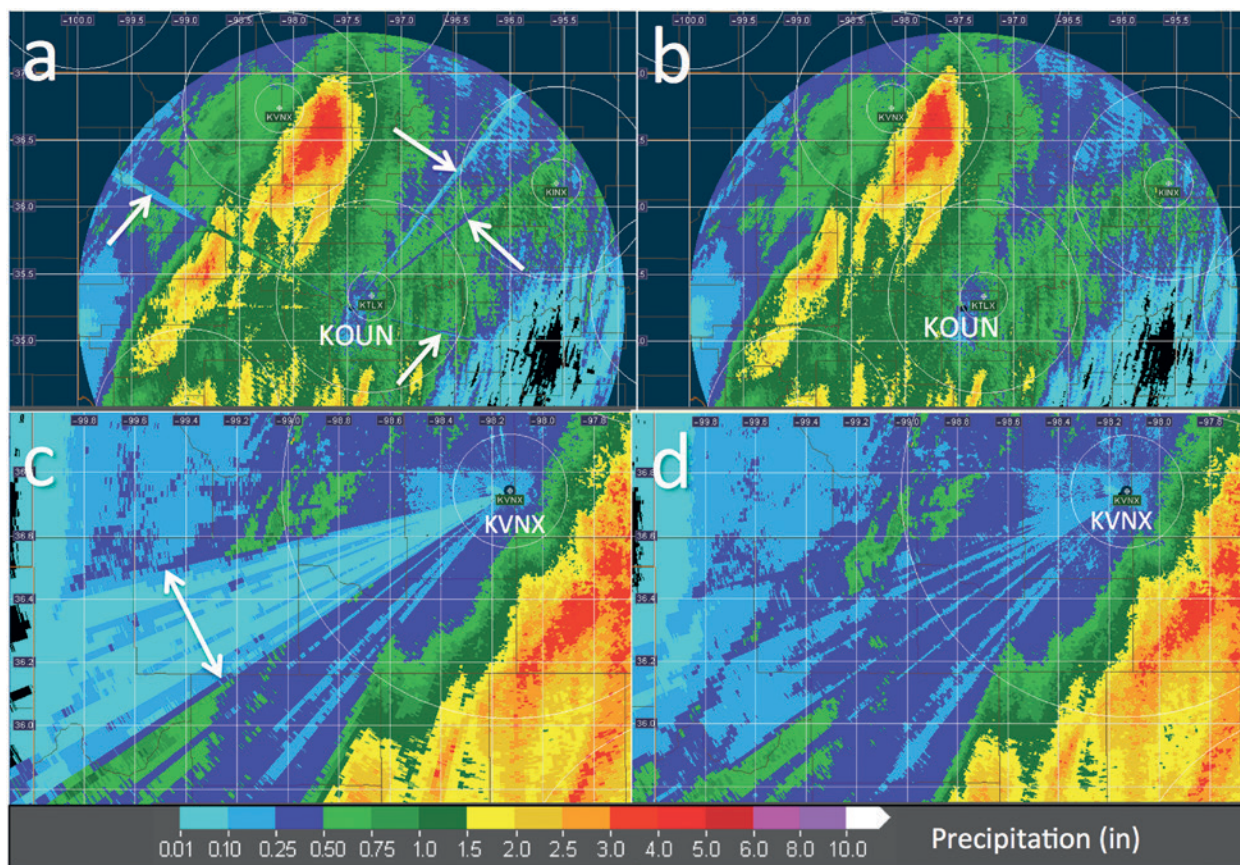


**FIG. 5.** Example QPE accumulation fields (a),(c) without the nonstandard blockage mitigation and (b),(d) with the mitigation. White arrows indicate areas of discontinuities due to blockages from cellphone and water towers in (a) and growing trees in (c).

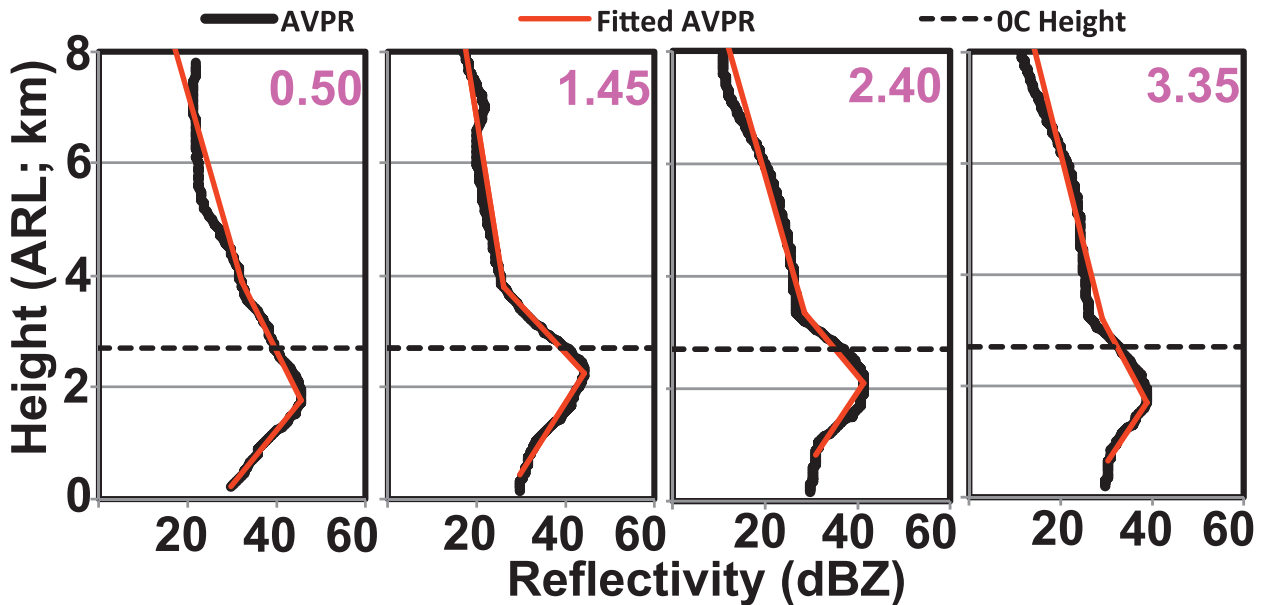


Fig. 6. AVPRs from KLWX radar at 1000 UTC 29 Oct 2012. Black curves represent radial profiles of azimuthal-mean reflectivities in stratiform precipitation areas on different tilts [pink numbers indicate elevation angles ( $^{\circ}$ )], and red lines are the linear-fitting AVPRs. Black dashed line shows  $0^{\circ}\text{C}$  height at the radar site, which was obtained from the RAP model analysis. The ordinate is height (km) above radar level (ARL).

The current AVPR correction does not work when the surface temperature is below  $0^{\circ}\text{C}$  because a reference level (BB bottom) would not be found. A climatological vertical profile of reflectivity (VPR)-based correction scheme similar to Koistinen and Pohjola (2014) is currently under development for enhancing the radar QPE in snow. Further, the correction usually works better on flat land than on complex terrain since the two assumptions (horizontal uniformity of vertical precipitation structure and invariant precipitation rate below BB bottom) are often violated in complex terrain, where orographic forcing modulates precipitation distributions (Zhang et al. 2012b).

The AVPR-corrected SHSR is derived from a single radar and then mosaicked onto the MRMS CONUS grid. Ideally, taking the lowest altitude datum among the multiple radars covering the same point would provide the most accurate surface precipitation rate estimate for the given point. However, such an approach inevitably introduces discontinuities in the QPE field midway between neighboring radars. The discontinuities may be due to different calibration biases among the radars and/or different beam propagation paths from the radars to the overlapping point. In MRMS, if the lowest (in altitude) SHSR datum shows no precipitation, then the mosaicked SHSR is set to no precipitation. This logic minimizes false precipitation introduced by radar observations of virga. Otherwise, the overlapping SHSR data are

grouped into “liquid,” “mixed,” and “ice” categories according to their heights with respect to the melting layer. If valid data are found in a lower-altitude group, then a weighted mean of those data are taken and the higher-altitude groups are ignored. This approach prevents usage of higher-altitude data in the SHSR mosaic when the lower-altitude data are available and allows a smooth transition across equidistant zones between neighboring radars. The mosaicking weight  $w_m$  is a product of two negative exponential functions—that is,  $w_m = \exp(-d^2/L^2)\exp(-h^2/H^2)$ , where  $d$  is the distance between the analysis point and the radar and  $h$  is the height of the single-radar SHSR bin;  $L$  and  $H$  are scaling factors with the default values of 100 and 2 km, respectively.

Seamless hybrid scan reflectivity height (SHSRH) product is the beam bottom height associated with SHSR data and is mosaicked onto the CONUS grid using the same logic as for SHSR. This field shows at every radar QPE grid point the height of radar observation from which the QPE is derived. Example SHSR and SHSRH fields from southeastern Oklahoma are shown in Fig. 8. A higher SHSRH area can be found south of the KSRX radar (Little Rock, Arkansas) (Fig. 8b), where the first tilt of KSRX was severely blocked and the second tilt was used in the hybrid scan. Generally, the higher the SHSRH, the lower the surface radar QPE accuracy as a result of various microphysical processes (e.g., melting, evaporation,



orographic precipitation enhancement) that could present below the hybrid scan. The SHSRH is a main contributing factor in the radar QPE quality index product that will be discussed next. SHSR and SHSRH are new national MRMS products and can provide useful information for meteorological and hydrological applications. For instance, the SHSR product has been used in a probabilistic QPE study recently (Kirstetter et al. 2015) that analyzed statistical relationships between the SHSR and surface gauge observations and generated different probabilistic QPE models for different precipitation types.

**RQI.** Radar QPEs are subject to various error sources, including 1) errors in radar measurements, for example, calibration biases and blockages; 2) contaminations from nonprecipitation echoes, for example, AP; 3) uncertainties in empirical relations between precipitation rate  $R$  and various radar variables (e.g., reflectivity  $Z$ ); and 4) variability in the VPR. Radar QPE quality index (RQI) has two multiplicative components, one is associated with beam blockages (error 1) and the another with beam spreading/ascending with range (error 4). The RQI blockage component has a value of one when there is no blockage and the value linearly decreases to zero when the beam blockage reaches a threshold (default = 50%). The range component has a value of one when the SHSR radar beam is completely below the melting layer, Fig. 9a). The 24-h radar QPE had a significant underestimation in the low RQI region. Meanwhile, some overestimation (area A) and underestimation (area B) were not reflected in RQI and may be due to other error factors not represented by the RQI (e.g., inaccurate  $R$ - $Z$  relationships).

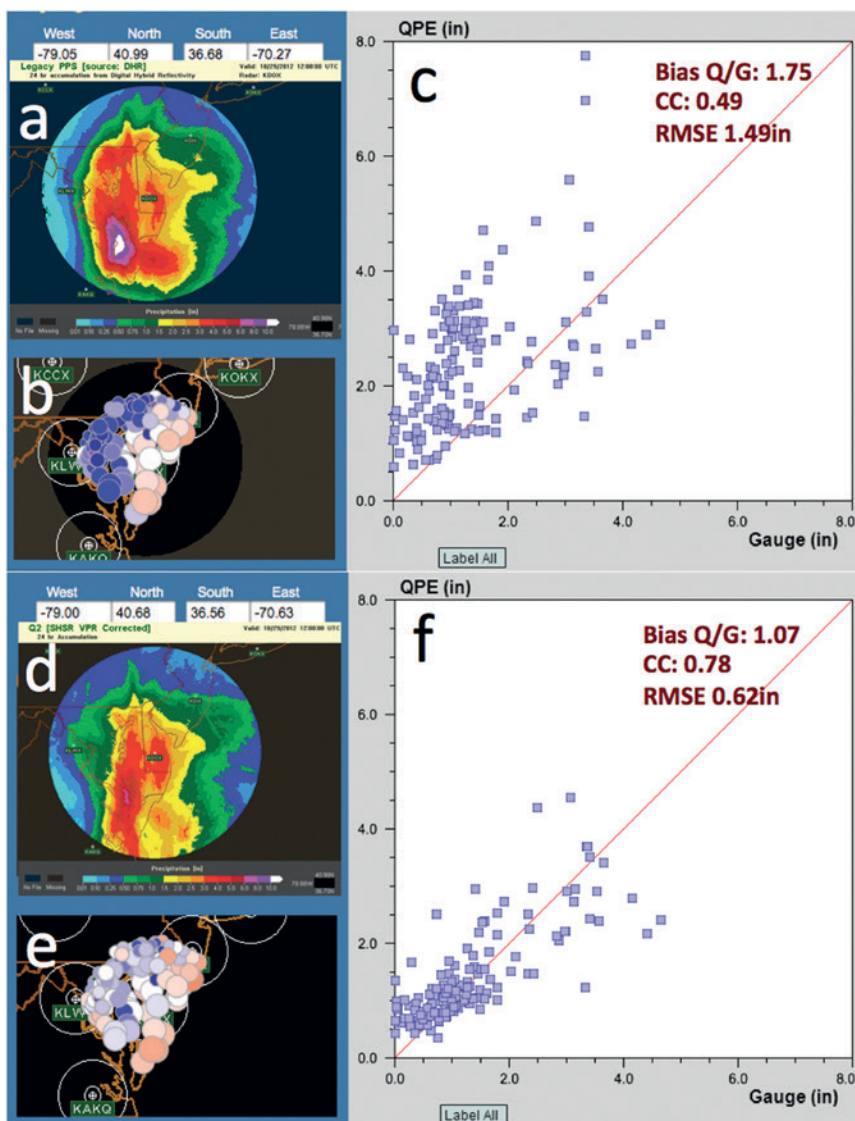


**FIG. 7.** Daily MRMS radar QPE maps (a) before and (d) after the AVPR correction. Bias ratios of the (b) QPEs vs (e) gauge observations are shown as the bubble charts. The size of the bubbles represents the gauge amounts, and the color represents the QPE bias (pink and red shadings indicate underestimation, and blue and purple shadings indicate overestimation). The associated scatterplots of the (c) QPEs vs (f) gauge data are also shown.

uncertainties in the radar QPE. However, RQI does not represent radar QPE uncertainties associated with spatially varying drop size distributions (error 3). Figure 9 shows an example RQI field where beam blockages and large distances between neighboring radars resulted in a low RQI (black dashed line, Fig. 9a). The 24-h radar QPE had a significant underestimation in the low RQI region. Meanwhile, some overestimation (area A) and underestimation (area B) were not reflected in RQI and may be due to other error factors not represented by the RQI (e.g., inaccurate  $R$ - $Z$  relationships).

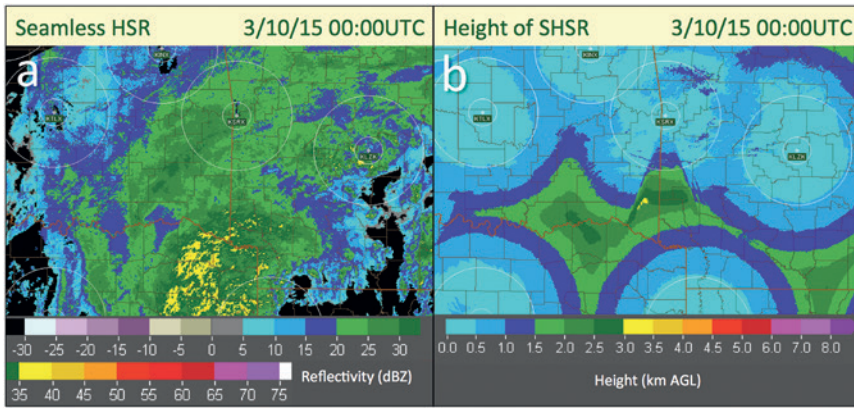


**FIG. 8.** Example (a) SHSR and (b) SHSRH fields valid at 1000 UTC 10 Mar 2015.

*Surface precipitation type (PCP\_FLAG).* Radar variables are indirect measurements of precipitation rates  $R$  and empirical relationships have to be developed for radar QPE. Different empirical relationships are needed for different precipitation phases and regimes, and an automated surface precipitation classification is employed in MRMS such that appropriate relationships may be applied. Figure 10 shows the MRMS surface precipitation classification process with seven categories (purple parallelograms in Fig. 10): 1) warm stratiform rain, 2) cool stratiform rain, 3) convective rain, 4) tropical-stratiform rain mix, 5) tropical-convective rain mix, 6) hail, and 7) snow. Snow areas are defined as where the surface temperature is below  $2^{\circ}\text{C}$  and the wet-bulb temperature is below  $0^{\circ}\text{C}$ . Areas with potential hail are determined by the maximum expected hail size, which is an MRMS severe weather product. Convective rain areas are identified through two steps: 1) the convective cores are identified based on high vertically integrated liquid (VIL, which is also an MRMS severe weather product) values and 2) the cores are then expanded with a composite reflectivity (CREF) criterion to obtain convective rain regions. A couple of constraints are applied during the convective core identification to avoid potential brightband areas.

Tropical rain identification is based on the methodology developed by Xu et al. (2008). For volume scan, a mean VPR is computed from full volume-scan reflectivity data near the radar (20–80-km range). The VPR (called “polar VPR”

$\geq 10^{\circ}\text{C}$ ), and the probability of warm rain (POWR; Grams et al. 2014) is high ( $\geq 0.5$ ). POWR was derived using decision trees based on a number of environmental predictors from the model analysis and is an indicator of the likelihood of enhanced precipitation rates as a result of the collision-coalescence process in an environment with a high freezing level and abundant moisture (Grams et al. 2014). The key predictors in the decision trees included 850–500-hPa temperature lapse rate, height of the freezing level, and 1000–700-hPa mean relative humidity. The POWR values range from 0 (low) to 1 (high) with high values corresponding to a moist adiabatic profile (i.e., weak lapse rate supporting weak updrafts), a high freezing level (deep warm layer for warm raindrop growth), and abundant low- to midlevel moisture (reduced evaporation of hydrometeors and/or low cloud bases). The tropical rain area is then expanded outside the predefined radius under the constraint of  $\text{SHSR} \geq 25 \text{ dBZ}$  and  $\text{POWR} \geq 0.5$ . Figure 11 shows an example surface precipitation type field valid at 2100 UTC

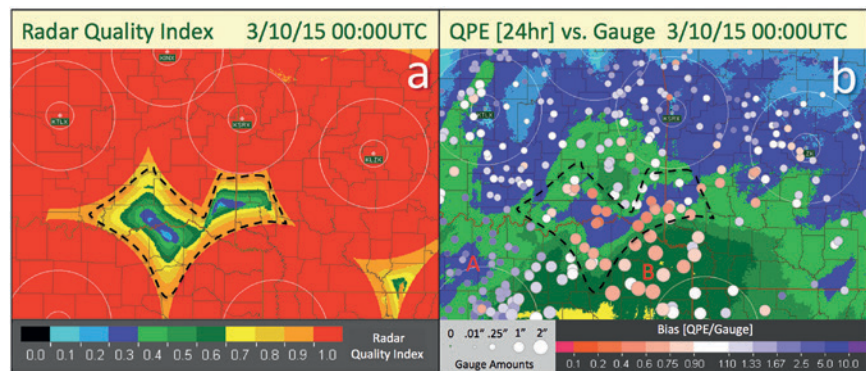


**FIG. 9.** Example RQI at (a) 0000 UTC 10 Mar 2015 and (b) a 24-h MRMS radar-only QPE accumulation ending at 0000 UTC 10 Mar 2015. In (b), the size of the solid circles represents the gauge-observed amounts, and the color of the circles represents the QPE/gauge bias ratio (red and pink shadings indicate underestimation, and blue and purple shadings indicate overestimation). The black dashed line indicates an area of low RQI.

21 December 2013, overlaid with surface observations from a crowdsourcing application called “the Meteorological Phenomena Identification Near the Ground” (mPING; Elmore et al. 2014). The snow line in the precipitation type field agreed well with the liquid–frozen precipitation boundary in mPING.

Surface precipitation rate (PCP\_RATE) and radar-only QPE (“Q3RAD”) accumulations. The MRMS surface precipitation rate is currently calculated using multiple R–Z relationships. Polarimetric variables are not used because various polarimetric radar QPE schemes are still under evaluation across CONUS and an optimal approach for all seasons and all geographic regions has yet to be developed. The following empirical R–Z relationships are used in MRMS to compute surface precipitation rate for each precipitation type:

warm and cold stratiform rain:

$$R_{\text{stra}} = \max(0.0365Z^{0.625}, 0.1155Z^{0.5}); \quad (1)$$

convective rain and hail:

$$R_{\text{conv}} = 0.017Z^{0.714}; \quad (2)$$

snow:

$$R_{\text{snow}} = 0.1155Z^{0.5}. \quad (3)$$

Here,  $Z$  represents the radar reflectivity ( $\text{mm}^6 \text{m}^{-3}$ ) and  $R$  represents rain rate [Eqs. (1) and (2)] or snow water equivalent [Eq. (3)] ( $\text{mm h}^{-1}$ ).

The two stratiform categories currently use the same combination of two R–Z relationships. However, a study similar to Kirstetter et al. (2015) is underway to assess variations of the R–Z relationship for the seven precipitation categories and new relationships may be developed. The categories are kept separate for potential R–Z scheme changes and/or the application of polarimetric radar QPE schemes

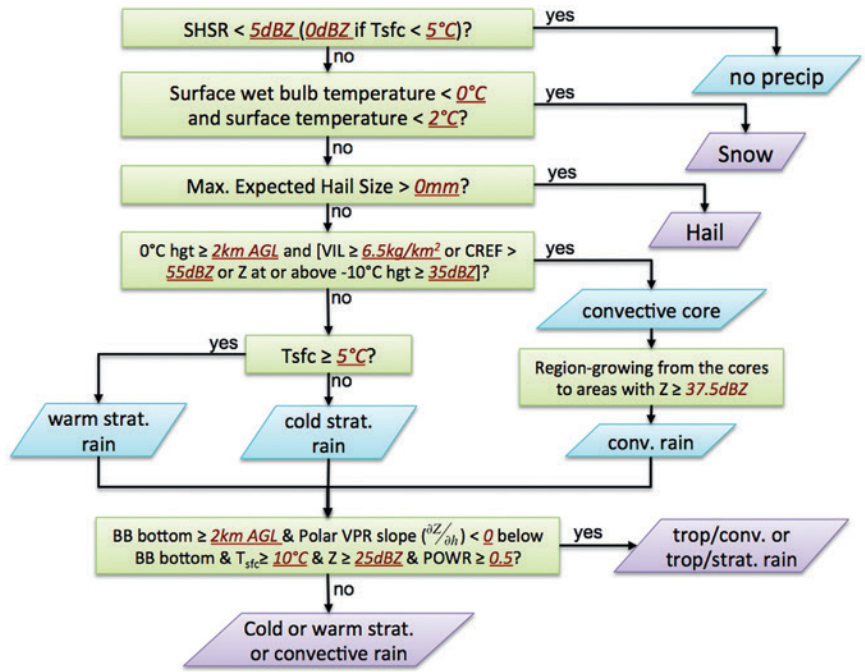


FIG. 10. The surface-precipitation-type classification process in the MRMS system. Underlined red fonts represent adaptable parameters in the classification algorithm.

in the future. The stratiform rain rates are currently capped at  $48.6 \text{ mm h}^{-1}$ , the convective rain is capped at  $103.8 \text{ mm h}^{-1}$ , and hail is capped at  $53.8 \text{ mm h}^{-1}$ .

The tropical–stratiform mixed rain rate  $R_{\text{tsmix}}$  is calculated as follows:

$$R_{\text{tsmix}} = \alpha w_{\text{trop}} R_{\text{trop}} + (1 - w_{\text{trop}}) R_{\text{stra}} \quad (4)$$

$$w_{\text{trop}} = \begin{cases} 0; & \text{POWR} \leq p_1 \\ \frac{\text{POWR} - p_1}{p_2 - p_1}; & p_1 < \text{POWR} \leq p_2 \\ 1; & \text{POWR} > p_2 \end{cases} \quad (5)$$

Here,  $R_{\text{stra}}$  represents a stratiform rain rate computed from Eq. (1),  $R_{\text{trop}} = 0.010Z^{0.833}$  represents a tropical rain rate (capped at  $147.4 \text{ mm h}^{-1}$ ),  $w_{\text{trop}}$  is the weight given to the tropical rain rate, and  $p_1$  and  $p_2$  are adaptable POWR thresholds (default values are  $p_1 = 0.5$  and  $p_2 = 0.7$  for June–November and  $p_1 = 0.75$  and  $p_2 = 1.0$  for December–May). The tropical rain-rate multiplier  $\alpha$  is defined as follows:

$$\alpha = \begin{cases} 1; & \text{POWR} \leq p_3 \\ 1 + (\alpha_{\text{max}} - 1) \frac{\text{POWR} - p_3}{p_4 - p_3}; & p_3 < \text{POWR} \leq p_4 \\ \alpha_{\text{max}}; & \text{POWR} > p_4 \end{cases} \quad (6)$$

where  $\alpha_{\max}$  varies from 1.1 to 1.5 during the hurricane season (June–November) and stays at 1.0 otherwise. Terms  $p_3$  and  $p_4$  are also adaptive parameters with default values of  $p_3 = 0.7$  and  $p_4 = 1.0$  for June–November and  $p_3 = 1.0$  and  $p_4 = 1.0$  for December–May. The tropical–convective mixed rain rate  $R_{\text{tcmix}}$  is calculated in the same way as in Eq. (4), except that  $R_{\text{stra}}$  is replaced by  $R_{\text{conv}}$ .

Note that Eqs. (4)–(6) are used for tropical–stratiform and tropical–convective rain rates in areas east of  $100^\circ\text{W}$  longitude, because the POWR was derived using data from only the eastern United States. The rates are simply set to  $R_{\text{trop}}$  west of  $102^\circ\text{W}$ . In the transition zone of  $102^\circ$ – $100^\circ\text{W}$ , a linear ramping of the two rates (i.e.,  $R_{\text{trop}}$  and  $R_{\text{tcmix}}$ , or  $R_{\text{trop}}$  and  $R_{\text{tcmix}}$ ) is applied to assure the continuity of the rate field. This scheme will undergo updating when a new POWR product becomes available for the western United States.

The rate field is calculated every 2 min and an hourly accumulation is computed every 2 min by aggregating the rate fields. Longer-term accumulations are then derived from the hourly accumulations at different update cycles (Table 1). It is noted that “skipping” patterns are sometimes observed in radar precipitation accumulation fields for fast-moving storms because of discrete temporal sampling of the storms by the radar. Such a pattern is more apparent in products with finer spatial resolution than those with coarser resolution owing to the spatial smoothing effects in the latter. Also, the patterns may be more apparent in single radar than in multiradar mosaic products because of additional observations in the latter.

Figure 12 shows CONUS mean absolute errors (MAEs) of daily MRMS radar–only QPE (blue line) and the NCEP stage-II (SII; Lin and Mitchell 2005) radar–only QPE (green line) with respect to the Community Collaborative Rain, Hail and Snow Network (CoCoRaHS: [www.cocorahs.org/](http://www.cocorahs.org/); Cifelli et al. 2005) gauges. Stage-II radar–only QPE is a national mosaic of the NWS operational single-polarization radar QPE (Fulton et al. 1998). Stage-II radar–only QPE uses one  $R$ – $Z$  relationship for each radar domain. Different  $R$ – $Z$  relationships may be used for different radars and the choice of using a single  $R$ – $Z$  relationship for each radar is set at the local forecast office level. The MRMS radar–only QPE showed consistent improvements over SII radar–only QPE throughout the year, likely because of impacts of several factors: 1) dual-polarization (MRMS) versus single-polarization (SII) reflectivity quality control, 2) spatially varying  $R$ – $Z$  relationships based on precipitation classification (MRMS) versus a single  $R$ – $Z$  relationship in a

radar domain (SII), 3) a VPR correction to mitigate radar QPE errors in bright band (MRMS) versus no VPR correction (SII), and 4) a conditional mosaicking scheme using negative exponential weighting functions of distance and height (MRMS) versus an inverse-distance-weighted mean mosaicking scheme (SII; [www.emc.ncep.noaa.gov/mmb/ylin/pcpanl/QandA/#INTROST2](http://www.emc.ncep.noaa.gov/mmb/ylin/pcpanl/QandA/#INTROST2)). The MRMS radar QPE had relatively large MAEs during June–October 2014 (Fig. 12) when compared to the CoCoRaHS gauges and the large errors were related to a wet bias in the MRMS QPE. The wet bias was partially due to inaccurate classifications of tropical rain areas in some continental convective systems, where the radar vertical profile of reflectivity and POWR showed characteristics similar to those in tropical storms. Other contributing factors included evaporation and advection of hydrometeors as they fall from the radar observation height to the ground and possibly gauge undercatch in severe storms with high winds.

*Local gauge bias-corrected radar QPE (“Q3GC”), gauge-only QPE, and gauge-influence index (GII).* Radar QPE provides a high-resolution and rapid update estimation of spatial precipitation distributions. However, uncertainties exist in the estimates because of imperfect empirical relationships between radar variables and precipitation rate and unknown processes below the lowest radar beam. Quality-controlled gauge observations provide direct and relatively more accurate estimates of precipitation amounts on the ground. A local gauge bias correction is made to the MRMS radar QPE to obtain a more accurate QPE, although at a latency ( $\sim 1.5$  h) because of the gauge data availability in real time. The local gauge bias correction is based on a method by Ware (2005) and involves three steps: 1) hourly radar–gauge differences are calculated at gauge stations, 2) the differences are interpolated onto the MRMS grid via an inverse-distance-weighted mean scheme, and 3) the interpolated difference field is subtracted from the hourly radar QPE field. The interpolation weight is in the form of  $w = 1/r^x$ , where  $w$  is the weight and  $r$  is the distance between a gauge and an MRMS grid point. Brandes (1975) used a negative exponential function in a similar study. The exponent  $x$  in the current scheme varies from 0.5 to 3 and is determined through cross validation that minimizes the interpolation error of radar–gauge differences in a specific domain each hour. The CONUS is divided into multiple subdomains (“tiles”) and the cross validation and local gauge correction of the radar QPE are performed for each tile. The corrected radar QPEs from all tiles at a given hour are then merged to

produce the final CONUS product.

The local gauge bias correction provided consistent improvements over the radar-only QPE throughout the year across the CONUS domain (Fig. 12). It is most effective in removing radar QPE errors that are spatially consistent since the interpolation weight is determined through the cross validation over a spatial domain. In the cool season (October–April) where precipitation is relatively widespread and homogeneous, the gauge-corrected radar QPE showed similar performances as the stage-IV product (Fig. 12), which

was a radar-, satellite-, gauge-, and PRISM-merged product generated by forecasters at RFCs with manual quality assurance. In the warm season (May–September), however, the MRMS gauge-corrected radar QPE still had larger errors than the stage-IV product (Fig. 12) when compared with CoCoRaHS gauges. The radar–gauge difference in the warm season varies significantly in space owing to a number of factors in convective storms, such as a high variability of drop size distributions, hydrometeor drifting and evaporation before reaching the ground, and gauge undercatch. The interpolated radar–gauge difference may not be representative of the radar QPE errors in areas away from the input gauges. Therefore, significant differences may still exist between the gauge-corrected radar QPE and the independent validation gauges. Also note that some of the CoCoRaHS gauges may have been used in stage IV but they are not used in the MRMS products.

The summation of weights from all gauges influencing a given grid point, normalized by the maximum value in the domain, is defined as the GII product. The same interpolation scheme was used to interpolate hourly gauge data to generate a gauge-only QPE. The hourly gauge-only and local gauge bias-corrected radar QPEs are aggregated to generate their longer-term accumulations.

*Mountain Mapper QPE (“Q3MM”).* Radar QPE quality in the Intermountain West suffers from severe terrain blockages. As a result, the RFCs in the west have been

using an alternative QPE called Mountain Mapper (Schaake et al. 2004). The same process is adopted in MRMS to generate a CONUS Mountain Mapper QPE. Mountain Mapper uses the PRISM monthly climatology as a background precipitation distribution map. Ratios between quality-controlled hourly gauge observations and collocated PRISM climatology values are calculated at each gauge station and the ratios are interpolated onto the MRMS grid using an inverse distance weighted mean ( $w = 1/r^2$ ). The MRMS Mountain Mapper QPE was found to provide consistent improvement over the MRMS radar QPE in the west and was applied in a multisensor-merged QPE (Zhang et al. 2014). A new multisensor-merged QPE using Mountain Mapper and the local gauge bias-corrected radar QPE is currently under evaluation and is planned for operational implementation in 2016.

**SUMMARY AND FUTURE WORK.** This paper provides an overview of the Multi-Radar Multi-Sensor (MRMS) system and its initial operating capabilities of quantitative precipitation estimation (QPE) products. MRMS was developed using severe weather product components from the Warning Decision Support System–Integrated Information (WDSS-II) and using QPE product components from the National Mosaic and Multi-Sensor QPE (NMQ) system. The system was transitioned into operations at the National Centers for Environmental Prediction in September 2014. It currently integrates

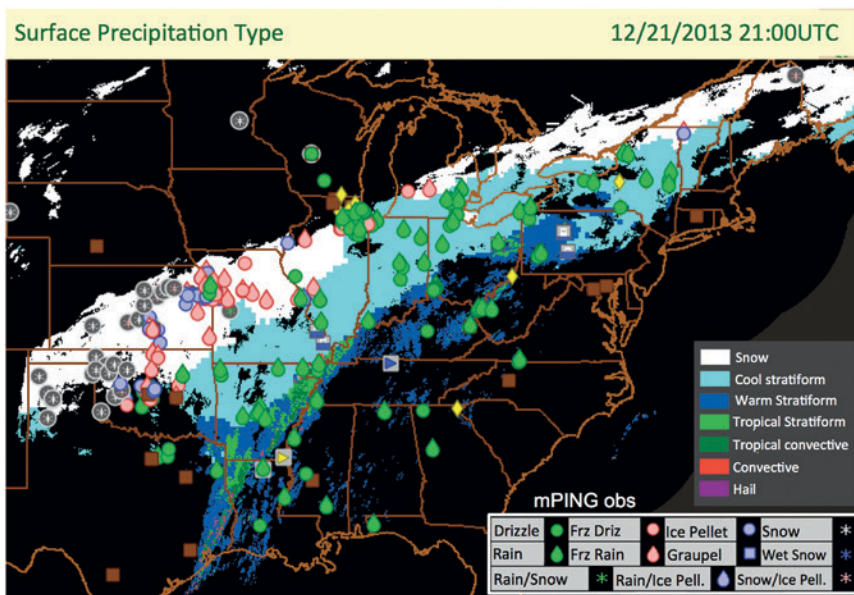


**FIG. 11. MRMS surface-precipitation-type product valid at 2100 UTC 21 Dec 2013. Surface observations of precipitation types from mPING are overlaid.**

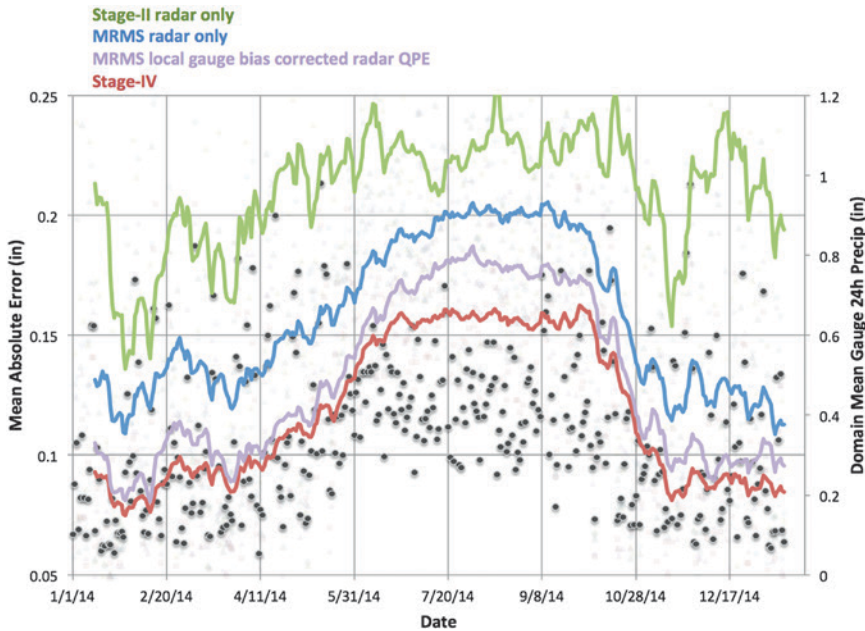


**FIG. 12. MAEs (left ordinate) of four QPE products with respect to CoCoRaHS gauge observations over the CONUS domain. The QPEs are 24-h accumulations ending at 1200 on each day for 2014. The black dots are domain-averaged daily precipitation observations from CoCoRaHS gauges (right ordinate).**

data from about 180 radars, about 7,000 gauges, and atmospheric environmental data in CONUS and southern Canada, and provides a suite of severe weather and QPE products at 1-km resolution and on a 2-min update cycle. Traditionally, operational radar products are generated at single-radar sites and then disseminated to regional or national centers. MRMS is a new paradigm in that the base-level data from all radars in a network are collected and processed at a centralized location. Such a process allows for easy integration of multisensor data and provides enhanced QPE products. Further, MRMS provides many new high-resolution national products, such as the 3D reflectivity mosaic, seamless hybrid scan reflectivity and associated height, and surface precipitation rate and type. These products have found many applications in the aviation, meteorological, and hydrological communities.

The MRMS surface precipitation rate is currently calculated using multiple  $R-Z$  relationships based on an automated surface precipitation classification. While the MRMS radar QPE showed consistent improvements over single  $R-Z$ -based radar QPEs over the CONUS, some challenges still remain. For instance, the current precipitation classification based on volume scan mean vertical profiles of reflectivity and probability of warm rain could misclassify some continental convective precipitation

as tropical rain and result in overestimations. On the other hand, the MRMS radar QPE underestimated some very heavy rain rates even though the tropical rain was correctly identified. Such underestimation appeared to be a result of attenuation, vertical variations of reflectivity, and/or unrepresentative  $R-Z$  relationships. The MRMS radar QPE still suffers from blockages in the complex terrain and may underestimate orographically enhanced precipitation. Many areas of CONUS have no radar coverage below 2 km above the ground level (Maddox et al. 2002) and the radar QPE in these areas is subject to uncertainties related to vertical variations

of reflectivity. Recent studies on the great Colorado flood of 2013 (e.g., Friedrich et al. 2016a,b; Gochis et al. 2015) also highlighted some of these challenges facing the radar QPE in the complex terrain. Further, the accuracy of MRMS radar QPE for frozen precipitation remains largely unknown on the hourly scale because of a lack of high-quality in situ snow water equivalent observations.

Polarimetric radar QPE using  $R-Z$ ,  $Z_{DR}$  (differential reflectivity) techniques (Giangrande and Ryzhkov 2008) showed advantages over the current MRMS in warm season (not shown) in the central and northern plains, where the MRMS has overestimations. However,  $R-Z$ ,  $Z_{DR}$  techniques were found to still have a dependency on precipitation regimes (Cunha et al. 2013; Ryzhkov et al. 2014) and they are sensitive to  $Z_{DR}$  calibration biases. The  $R$ -specific differential phase  $K_{DP}$  (e.g., Bringi and Chandrasekar 2001; Ryzhkov et al. 2005; Matrosov 2010; Wang and Chandrasekar 2010; Lim et al. 2013) and  $R$ -specific attenuation  $A$  (e.g., Ryzhkov et al. 2014; Wang et al. 2014) schemes were shown to have advantages over  $R-Z$  and  $R-Z$ ,  $Z_{DR}$  because  $K_{DP}$  and  $A$  are immune to calibration biases and to partial beam blockages. However, the  $R-K_{DP}$  and  $R-A$  schemes cannot be used in regions of frozen or mixed phases of hydrometeors and their performance in light and/or scattered precipitation is not as robust as in widespread heavy rain. Therefore, a

synthetic  $R-A$ ,  $R-K_{DP}$ , and  $R-Z$  radar QPE is currently under development in MRMS. The new synthetic dual-polarization radar QPE will apply  $R-A$  in areas of widespread rain,  $R-K_{DP}$  in areas of hail or rain-hail mix, and a VPR-corrected  $R-Z$  in areas with frozen and mixed-phase precipitation. The new scheme is planned for implementation in the operational MRMS system by the end of 2016 and is expected to improve the MRMS radar QPE in the warm season.

To facilitate the rapid and seamless research-to-operations transfer of advanced radar technologies, a real-time research MRMS system is deployed at the National Severe Storms Laboratory. The system serves as a national test bed for new multiradar multisensor QPE technologies and includes a web-based QPE verification system (QVS; <http://mrms.ou.edu>). QVS provides a variety of statistical tools and screening procedures for viewing and analyzing MRMS products and incoming datasets from a few minutes to a couple of years old. One focus of the QVS is the QPE products verification, including 2D maps of color-coded QPE/gauge ratios and gauge amount circles, scatterplots, and multivariable time series plots for any point in the entire MRMS grid. Many users from NWS forecast offices, universities, and private sectors have used QVS and have provided invaluable feedback based on real-time (real world) evaluations that guided MRMS development to what it is today and for the future.

**ACKNOWLEDGMENTS.** Major funding for this research was provided under the agreement between the National Oceanic and Atmospheric Administration (NOAA) and the American Institute in Taiwan (AIT) and the agreement between NOAA and the Salt River Project. Partial funding was provided under NOAA–University of Oklahoma Cooperative Agreements NA17RJ1227 and NA13OAR4830236. The NOAA Integrated Dissemination Program and the National Weather Service’s Office of Science and Technology program provided additional support and computational resources.

## REFERENCES

Brandes, E. A., 1975: Optimizing rainfall estimates with the aid of radar. *J. Appl. Meteor.*, **14**, 1339–1345, doi:10.1175/1520-0450(1975)014<1339:OREWTA>2.0.CO;2.

Brangi, V. N., and V. Chandrasekar, 2001: *Polarimetric Doppler Weather Radar: Principles and Applications*. Cambridge University Press, 636 pp.

Chen, S., and Coauthors, 2013: Evaluation and uncertainty estimation of NOAA/NSSL next-generation National Mosaic QPE (Q2) over the continental

United States. *J. Hydrometeor.*, **14**, 1308–1322, doi:10.1175/JHM-D-12-0150.1.

Cifelli, R., N. Doesken, P. Kennedy, L. D. Carey, S. A. Rutledge, C. Gimmestad, and T. Depue, 2005: The Community Collaborative Rain, Hail, and Snow Network: Informal education for scientists and citizens. *Bull. Amer. Meteor. Soc.*, **86**, 1069–1077, doi:10.1175/BAMS-86-8-1069.

Cunha, L. K., J. A. Smith, M. L. Baeck, and W. F. Krajewski, 2013: An early performance evaluation of the NEXRAD dual-polarization radar rainfall estimates for urban flood applications. *Wea. Forecasting*, **28**, 1478–1497, doi:10.1175/WAF-D-13-00046.1.

Daly, C. R., P. Neilson, and D. L. Phillips, 1994: A statistical-topographic model for mapping climatological precipitation over mountainous terrain. *J. Appl. Meteor.*, **33**, 140–158, doi:10.1175/1520-0450(1994)033<0140:ASTMFM>2.0.CO;2.

—, M. Halbleib, J. I. Smith, W. P. Gibson, M. K. Doggett, G. H. Taylor, J. Curtis, and P. P. Pasteris, 2008: Physiographically sensitive mapping of climatological temperature and precipitation across the conterminous United States. *Int. J. Climatol.*, **28**, 2031–2064, doi:10.1002/joc.1688.

Diffendorfer, J. E., R. Compton, L. Kramer, Z. Ancona, and D. Norton, 2014: Onshore industrial wind turbine locations for the United States through July 2013. U.S. Geological Survey Data Series 817. [Available online at <http://pubs.usgs.gov/ds/817/>.]

Droegemeier, K. K., and Coauthors, 2002: Project CRAFT: A test bed for demonstrating the real time acquisition and archival of WSR-88D level II data. Preprints, *18th Int. Conf. on Interactive Information Processing Systems for Meteorology, Oceanography, and Hydrology*, Orlando, FL, Amer. Meteor. Soc., 5.20. [Available online at <https://ams.confex.com/ams/annual2002/webprogram/Paper30900.html>.]

Elmore, K., Z. Flamig, V. Lakshmanan, B. Kaney, V. Farmer, H. Reeves, and L. Rothfus, 2014: mPING: Crowd-sourcing weather reports for research. *Bull. Amer. Meteor. Soc.*, **95**, 1335–1342, doi:10.1175/BAMS-D-13-00014.1.

Essery, C. I., and D. N. Wilcock, 1991: The variation in rainfall catch from standard UK Meteorological Office raingauges: A twelve year case study. *Hydrol. Sci. J.*, **36**, 23–34, doi:10.1080/02626669109492482.

Friedrich, K., E. Kalina, J. Aikins, D. Gochis, and R. Rasmussen, 2016a: Precipitation and cloud structures of intense rain during the 2013 Great Colorado Flood. *J. Hydrometeor.*, **17**, 27–52, doi:10.1175/JHM-D-14-0157.1.

—, —, —, M. Steiner, D. Gochis, P. Kucera, K. Ikeda, and J. Sun, 2016b: Raindrop size distribution

- and rain characteristics during the 2013 Great Colorado Flood. *J. Hydrometeor.*, **17**, 27–52, doi:10.1175/JHM-D-14-0184.1.
- Fulton, R., J. Breidenbach, D.-J. Seo, D. Miller, and T. O'Bannon, 1998: The WSR-88D rainfall algorithm. *Wea. Forecasting*, **13**, 377–395, doi:10.1175/1520-0434(1998)013<0377:TWRA>2.0.CO;2.
- Giangrande, S. E., and A. V. Ryzhkov, 2008: Estimation of rainfall based on the results of polarimetric echo classification. *J. Appl. Meteor. Climatol.*, **47**, 2445–2462, doi:10.1175/2008JAMC1753.1.
- Gochis, D., and Coauthors, 2015: The great Colorado flood of September 2013. *Bull. Amer. Meteor. Soc.*, **96**, 1461–1487, doi:10.1175/BAMS-D-13-00241.1.
- Grams, H., J. Zhang, and K. Elmore, 2014: Automated identification of enhanced rainfall rates using the near-storm environment for radar precipitation estimates. *J. Hydrometeor.*, **15**, 1238–1254, doi:10.1175/JHM-D-13-042.1.
- Groisman, P. Ya., and D. R. Legates, 1994: The accuracy of United States precipitation data. *Bull. Amer. Meteor. Soc.*, **75**, 215–227, doi:10.1175/1520-0477(1994)075<0215:TAO USP>2.0.CO;2.
- Kelleher, K. E., and Coauthors, 2007: Project CRAFT: A real-time delivery system for NEXRAD level II data via the Internet. *Bull. Amer. Meteor. Soc.*, **88**, 1045–1057, doi:10.1175/BAMS-88-7-1045.
- Kirstetter, P.-E., J. J. Gourley, Y. Hong, J. Zhang, S. Moazamigoodarzi, C. Langston, and A. Arthur, 2015: Probabilistic precipitation rate estimates with ground-based radar network. *Water Resour. Res.*, **51**, 1422–1442, doi:10.1002/2014WR015672.
- Koistinen, J., and H. Pohjola, 2014: Estimation of ground-level reflectivity factor in operational weather radar networks using VPR-based correction ensembles. *J. Appl. Meteor. Climatol.*, **53**, 2394–2411, doi:10.1175/JAMC-D-13-0343.1.
- Lakshmanan, V., T. Smith, G. J. Stumpf, and K. Hondl, 2007: The Warning Decision Support System–Integrated Information. *Wea. Forecasting*, **22**, 596–612, doi:10.1175/WAF1009.1.
- , J. Zhang, K. Hondl, and C. Langston, 2012: A statistical approach to mitigating persistent clutter in radar reflectivity data. *IEEE J. Sel. Top. Appl. Earth Obs. Remote Sens.*, **5**, 652–662, doi:10.1109/JSTARS.2011.2181828.
- Larson, L. W., and E. L. Peck, 1974: Accuracy of precipitation measurements for hydrologic modeling. *Water Resour. Res.*, **10**, 857–863, doi:10.1029/WR010i004p00857.
- Lim, S., R. Cifelli, V. Chandrasekar, and S. Matrosov, 2013: Precipitation classification and quantification using X-band dual-polarization weather radar: Application in the Hydrometeorology Testbed. *J. Atmos. Oceanic Technol.*, **30**, 2108–2120, doi:10.1175/JTECH-D-12-00123.1.
- Lin, Y., and K. E. Mitchell, 2005: The NCEP stage II/IV hourly precipitation analyses: Development and applications. *19th Conf. on Hydrology*, San Diego, CA, Amer. Meteor. Soc., 1.2. [Available online at [https://ams.confex.com/ams/Annual2005/techprogram/paper\\_83847.htm](https://ams.confex.com/ams/Annual2005/techprogram/paper_83847.htm).]
- Maddox, R. A., J. Zhang, J. J. Gourley, and K. W. Howard, 2002: Weather radar coverage over the contiguous United States. *Wea. Forecasting*, **17**, 927–934, doi:10.1175/1520-0434(2002)017<0927:WR COTC>2.0.CO;2.
- Matrosov, S. Y., 2010: Evaluating polarimetric X-band radar rainfall estimators during HMT. *J. Atmos. Oceanic Technol.*, **27**, 122–134, doi:10.1175/2009JTECHA1318.1.
- Parsons, D. A., 1941: Calibration of a Weather Bureau tipping-bucket gage. *Mon. Wea. Rev.*, **69**, 205–208, doi:10.1175/1520-0493(1941)069<0205:COAWBT>2.0.CO;2.
- Qi, Y., J. Zhang, and P. Zhang, 2013a: A real-time automated convective and stratiform precipitation segregation algorithm in native radar coordinates. *Quart. J. Roy. Meteor. Soc.*, **139**, 2233–2240, doi:10.1002/qj.2095.
- , —, —, and Q. Cao, 2013b: VPR correction of bright band effects in radar QPEs using polarimetric radar observations. *J. Geophys. Res. Atmos.*, **118**, 3627–3633, doi:10.1002/jgrd.50364.
- Rasmussen, R., and Coauthors, 2012: How well are we measuring snow: The NOAA/FAA/NCAR winter precipitation test bed. *Bull. Amer. Meteor. Soc.*, **93**, 811–829, doi:10.1175/BAMS-D-11-00052.1.
- Ryzhkov, A. V., T. J. Schuur, D. W. Burgess, P. L. Heinselman, S. Giangrande, and D. S. Zrnić, 2005: The Joint Polarization Experiment polarimetric rainfall measurements and hydrometeor classification. *Bull. Amer. Meteor. Soc.*, **86**, 809–824, doi:10.1175/BAMS-86-6-809.
- , M. Diederich, P. Zhang, and C. Simmer, 2014: Potential utilization of specific attenuation for rainfall estimation, mitigation of partial beam blockage, and radar networking. *J. Atmos. Oceanic Technol.*, **31**, 599–619, doi:10.1175/JTECH-D-13-00038.1.
- Schaake, J., A. Henkel, and S. Cong, 2004: Application of PRISM climatologies for hydrologic modeling and forecasting in the western U.S. *18th Conf. on Hydrology*, Seattle, WA, Amer. Meteor. Soc., 5.3. [Available online at [https://ams.confex.com/ams/84Annual/techprogram/paper\\_72159.htm](https://ams.confex.com/ams/84Annual/techprogram/paper_72159.htm).]
- Sevruk, B., 2005: Rainfall measurement: Gauges. *Encyclopedia of Hydrological Sciences*, M. G. Anderson, Ed., John Wiley & Sons Ltd., 529–536.

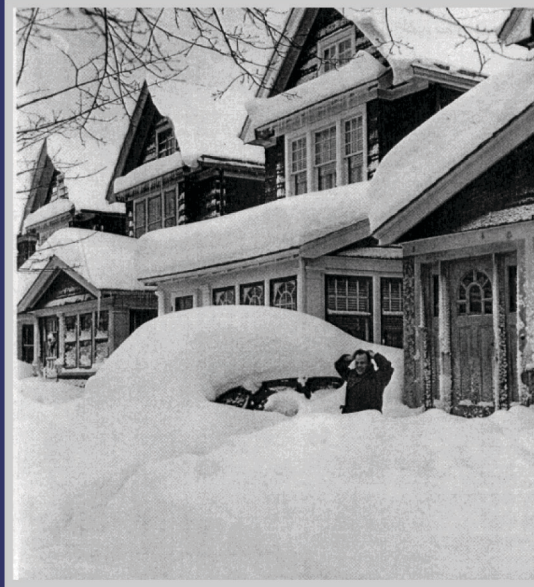


- Sieck, L. C., S. J. Burges, and M. Steiner, 2007: Challenges in obtaining reliable measurements of point rainfall. *Water Resour. Res.*, **43**, W01420, doi:10.1029/2005WR004519.
- Smith, T. M., and Coauthors, 2016: Multi-Radar Multi-Sensor (MRMS) Severe weather and aviation products: Initial operating capabilities. *Bull. Amer. Meteor. Soc.*, doi:10.1175/BAMS-D-14-00173.1, in press.
- Tang, L., J. Zhang, Y. Qi, C. Langston, and K. W. Howard, 2013: Non-standard blockage mitigation for national radar QPE products. *36th Conf. on Radar Meteorology*, Breckenridge, CO, Amer. Meteor. Soc., 354. [Available online at <https://ams.confex.com/ams/36Radar/webprogram/Paper228659.html>.]
- , —, C. Langston, J. Krause, K. Howard, and V. Lakshmanan, 2014: A physically based precipitation–nonprecipitation radar echo classifier using polarimetric and environmental data in a real-time national system. *Wea. Forecasting*, **29**, 1106–1119, doi:10.1175/WAF-D-13-00072.1.
- Wang, Y. D., P. Zhang, A. Ryzhkov, J. Zhang, and P.-L. Chang, 2014: Utilization of specific attenuation for tropical rainfall estimation in complex terrain. *J. Hydrometeorol.*, **15**, 2250–2266, doi:10.1175/JHM-D-14-0003.1.
- Wang, Y. T., and V. Chandrasekar, 2010: Quantitative precipitation estimation in the CASA X-band dual-polarization radar network. *J. Atmos. Oceanic Technol.*, **27**, 1665–1676, doi:10.1175/2010JTECHA1419.1.
- Ware, E. C., 2005: Corrections to radar-estimated precipitation using observed rain gauge data. M.S. thesis, Cornell University, 96 pp. [Available online at <https://ecommons.cornell.edu/bitstream/1813/2115/1/pdfthesis.pdf>.]
- Xu, X., K. Howard, and J. Zhang, 2008: An automated radar technique for the identification of tropical precipitation. *J. Hydrometeorol.*, **9**, 885–902, doi:10.1175/2007JHM954.1.
- Zhang, J., and Y. Qi, 2010: A real-time algorithm for the correction of brightband effects in radar-derived QPE. *J. Hydrometeorol.*, **11**, 1157–1171, doi:10.1175/2010JHM1201.1.
- , and Coauthors, 2011: National Mosaic and Multi-Sensor QPE (NMQ) system: Description, results, and future plans. *Bull. Amer. Meteor. Soc.*, **92**, 1321–1338, doi:10.1175/2011BAMS-D-11-00047.1.
- , Y. Qi, K. Howard, C. Langston, and B. Kaney, 2012a: Radar Quality Index (RQI)—A combined measure for beam blockage and VPR effects in a national network. *Weather Radar and Hydrology*, R. J. Moore, S. J. Cole, and A. J. Illingworth, Eds., IAHS Publ. 351, 388–393.
- , —, D. Kingsmill, and K. Howard, 2012b: Radar-based quantitative precipitation estimation for the cool season in complex terrain: Case studies from the NOAA Hydrometeorology Testbed. *J. Hydrometeorol.*, **13**, 1836–1854, doi:10.1175/JHM-D-11-0145.1.
- , —, B. Kaney, C. Langston, and K. Howard, 2014: A real-time algorithm for merging radar QPEs with rain gauge observations and orographic precipitation climatology. *J. Hydrometeorol.*, **15**, 1794–1809, doi:10.1175/JHM-D-13-0163.1.



# NORTHEAST SNOWSTORMS

Volume I: Overview



PAUL J. KOCIN & LOUIS W. UCCELLINI  
Published by the American Meteorological Society



# NORTHEAST SNOWSTORMS

Volume I: Overview  
Volume II: The Cases

Paul J. Kocin and Louis W. Uccellini

*Northeast Snowstorms* offers the most comprehensive treatment on winter storms ever compiled: more than 50 years of professional experience in the form of a two-volume compendium of insights, examples, photographs, over 200 color figures, and a DVD of added material.

American Meteorological Society; 818 pages, hardbound;  
AMS code MM54

Price: \$100.00 list/\$80.00 member/ \$60.00 student member

### ORDER ONLINE!

[www.ametsoc.org/amsbookstore](http://www.ametsoc.org/amsbookstore)

or see the order form at the back of this issue.



Copyright of Bulletin of the American Meteorological Society is the property of American Meteorological Society and its content may not be copied or emailed to multiple sites or posted to a listserv without the copyright holder's express written permission. However, users may print, download, or email articles for individual use.